ACS APPLIED MATERIALS & INTERFACES

www.acsami.org

Research Article

# $SO_2$ Capture by Two Aluminum-Based MOFs: Rigid-like MIL-53(Al)-TDC *versus* Breathing MIL-53(Al)-BDC

Alfredo López-Olvera,[¶] J. Antonio Zárate,[¶] Eva Martínez-Ahumada, Dong Fan, Mariana L. Díaz-Ramírez, Paola A. Sáenz-Cavazos, Vladimir Martis, Daryl R. Williams, Elí Sánchez-González, Guillaume Maurin,* and Ilich A. Ibarra*

Cite This: *ACS Appl. Mater. Interfaces* 2021, 13, 39363−39370

Read Online

ACCESS | Metrics & More | Article Recommendations | Supporting Information

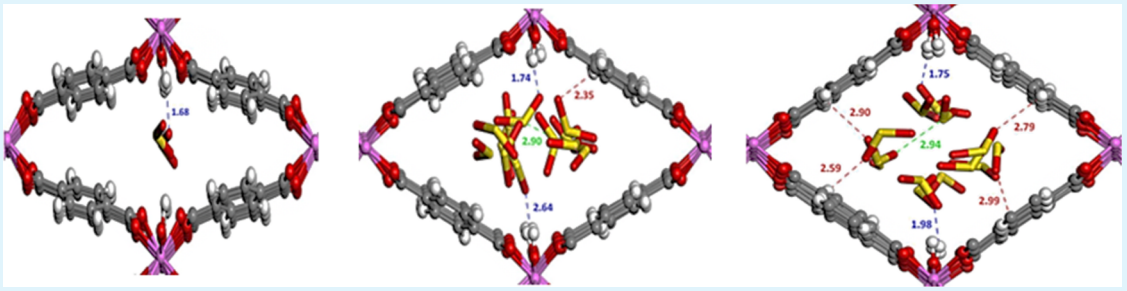


**ABSTRACT:** Metal−organic frameworks MIL-53(Al)-TDC and MIL-53(Al)-BDC were explored in the $SO_2$ adsorption process. MIL-53(Al)-TDC was shown to behave as a rigid-like material upon $SO_2$ adsorption. On the other hand, MIL-53(Al)-BDC exhibits guest-induced flexibility of the framework with the presence of multiple steps in the $SO_2$ adsorption isotherm that was related through molecular simulations to the existence of three different pore opening phases narrow pore, intermediate pore, and large pore. Both materials proved to be exceptional candidates for $SO_2$ capture, even under wet conditions, with excellent $SO_2$ adsorption, good cycling, chemical stability, and easy regeneration. Further, we propose MIL-53(Al)-TDC and MIL-53(A)-BDC of potential interest for $SO_2$ sensing and $SO_2$ storage/transportation, respectively.

**KEYWORDS:** *$SO_2$ capture, MOFs, breathing, adsorption measurements, molecular modeling*



## 1. INTRODUCTION

Air quality is nowadays a major concern in our modern society. In 2018, the U.S. Environmental Protection Agency identified and grouped six common air pollutants that can severely affect human health: (1) carbon monoxide (CO), (2) sublimated lead (Pb), (3) nitrogen oxides ($NO_x$), (4) ozone ($O_3$), (5) particulate matter (PM10/2.5), and (6) sulfur oxides ($SO_x$).[1] Particularly, $SO_2$ is a colorless and hazardous gas with suppressing odor that can trigger several respiratory issues, for example, chronic bronchitis and laryngitis.[2] In fact, the World Health Organization fixed the $SO_2$ exposure limit to about 10 ppm over 10 min per day, and a concentration above 100 ppm could be lethal for humans.[3] Lower $SO_2$ concentrations (between 2 and 3 ppm) can also have a devastating impact on our environment and vegetation. Even though natural $SO_2$ discharge occurs as a byproduct of volcanic eruptions, to date, more than 80% of the $SO_2$ released into the atmosphere is produced by two main anthropogenic sources, that is, stationary fuel combustion and industrial process.[4] Therefore there is a crucial need to implement remediation systems for substantially reducing $SO_2$ concentration in air.

Over the past years, several techniques have been developed for $SO_2$ removal from industrial processes, for example, $SO_2$ fixation as disulfitomercurate[5,6] (a compound with high toxicity in low amounts) and the flue gas desulfurization (FGD) process. FGD consists of two main steps: the single-use process and the recovery system. For the latter, the standard sorbents are expensive scrubbers in alkaline medium, that is, lime or limestone, sodium hydroxide, ammonium, and seawater, among others.[7,8] On top of that, only 10% of the recovered $SO_2$ can be used for other purposes such as industrial conversion of $SO_2$ to sulfuric acid.[9,10] Another alternative to remove $SO_2$ from natural gas is the use of porous solids such as zeolites, metal oxides, and activated carbons.[10−13] However, it was shown that this series of adsorbents captures $SO_2$ mostly through chemisorption, implying high recovery costs due to the necessary high temperatures or pressures and the use of long chemical

Received: May 28, 2021
Accepted: July 27, 2021
Published: August 11, 2021

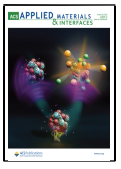




https://doi.org/10.1021/acsami.1c09944
*ACS Appl. Mater. Interfaces* 2021, 13, 39363−39370

treatments.[14−16] Developing new $SO_2$ sorbent materials with high adsorption capacity, stability, and easy regeneration has become a critical requirement.

Metal−organic frameworks (MOFs) or porous coordination polymers are one of the most recent classes of crystalline micro-/mesoporous materials formed by the assembly of metal ions/metal oxide clusters and a series of organic linkers (carboxylate, azolate, phenolate, *etc.*). Most of these MOFs are chemically and thermally stable and have aroused tremendous interests in diverse areas[17] including gas separation,[18−22] gas storage,[23−25] ion exchange,[26−28] chemical sensing,[29−32] drug delivery,[33−35] and catalysis,[36−38] among others. More specifically, a series of MOFs was demonstrated to be able to capture corrosive and hazardous gases such as $H_2S$ and $SO_2$; however, some of them exhibit limited stability toward these contaminants.[39−41] Typically, $Ba_{0.5}[Ni_8(OH)_3(EtO)_3(BPD\_NH_2)_{5.5}]$,[42] MIL-125(Ti)−$NH_2$,[43] and MOF-177[44] show high $SO_2$ adsorption capacities (5.6, 7.9, and 25.7 mmol $g^{-1}$, respectively) but suffer from structural degradation upon exposure to this toxic gas. In particular, the structural stability of MOFs in wet $SO_2$ conditions [50−65% relative humidity (RH)] is a fundamental concern.[45] Some MOF materials such as MFM-202a,[46] M-MOF-74 (M = Zn(II) and Ni(II)),[47,48] and MIL-125(Ti)−$NH_2$[43] exhibit high $SO_2$ uptakes; however, the concomitant presence of water was shown to play a detrimental role in their stability and their $SO_2$ uptake performance. Conversely, some of us recently demonstrated a high chemical stability of MIL-101(Cr)−4F(1%) upon wet $SO_2$ adsorption.[25,49] Several Al(III)-based MOFs, for example, MIL-160,[44] MFM-305,[50] MFM-300(Al),[51] and CAU-10,[52] have equally shown high stability to $SO_2$ and good $SO_2$ capture performances under atmospheric conditions, that is, 7.2, 6.9, 8.1, and 4.5 mmol $g^{-1}$, respectively. Further, the last two materials[51,52] have demonstrated high cyclability (up to 50 adsorption−desorption cycles) and structural stability under wet $SO_2$.

MIL-53(Al)-BDC (BDC = 1,4 benzene dicarboxylate)[53] is a well-known flexible MOF material constructed by infinite chains of trans-corner-sharing $[AlO_4(\mu\text{-}OH)_2]$ octahedral and cross-linked by 1,4 BDC linkers, which has demonstrated attractive gas adsorption properties owing to its guest-induced breathing behavior.[54−60] The thiophene analogue MIL-53(Al)-TDC (TDC = 2,5-thiophenedicarboxylate) first reported by Stock and co-workers in 2017[61] has been investigated for heat transformation applications,[62] capture of hazardous gases ($CO_2$ and $H_2S$),[63] and very recently, $I_2$ detection.[64] Thus, we anticipated MIL-53(Al)-TDC to behave as a rigid structure upon $SO_2$ adsorption, as previously demonstrated for other probe molecules, for example, $CO_2$, $H_2S$, $N_2$, $CH_4$, $H_2O$, and EtOH,[61−64] exhibiting potentially attractive $SO_2$ uptake performance compared to other representative MOF materials such as MIL-101(Cr)−4F(1%),[49] MIL-160,[44] MFM-300-(Al),[51] and CAU-10.[52] Additionally, we hypothesized that MIL-53(Al)-BDC should also show promising $SO_2$ uptake performance, however, associated with a flexible adsorption-induced structural behavior upon the whole adsorption process, which is of fundamental interest for further applications. Herein, we report the $SO_2$ adsorption properties of these two Al(III)-based MOFs, MIL-53(Al)-TDC and MIL-53(Al)-BDC (see Scheme 1). Our hybrid experimental−computational approach demonstrated a rigid-like behavior of MIL-53(Al)-TDC upon adsorption, although a spectacular multistep adsorption was evidenced for MIL-53(Al)-BDC, and this was assigned to three subsequent structural transitions between narrow, intermediate, and large pore forms. Interestingly these two Al-MOFs were shown to be highly stable upon $SO_2$ adsorption even under wet conditions (60% RH) while maintaining a high level of capture performance upon cycling.

**Scheme 1. Organic Ligands Used in Both (a) MIL-53(Al)-TDC and (b) MIL-53(Al)-BDC Materials: TDC and BDC, Respectively**[a]

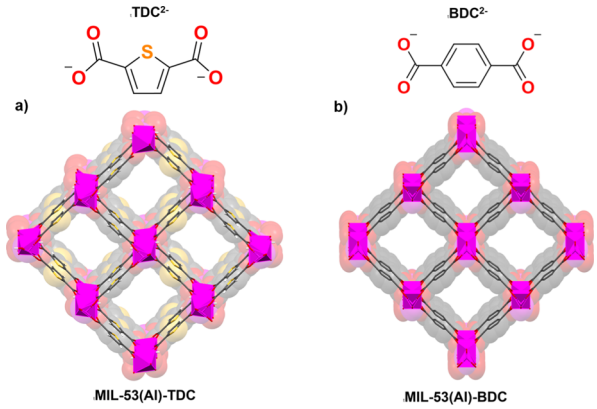


[a]View along the *b*-axis of rhombohedral-shape pores in the MIL-53(Al) topology, pink octahedral: $AlO_4(\mu\text{-}OH)_2$; red: oxygen; black: carbon, and sulfur yellow.

## 2. RESULTS AND DISCUSSION

**2.1. Synthesis and Characterization.** According to the literature,[61] MIL-53(Al)-TDC was synthetized by the hydrothermal reaction between $H_2$TDC and $AlCl_3$ (1:1.3 ratio, respectively) in a DMF/$H_2O$ mixture at 100 °C during 5 h (see Supporting Information). Similarly, the hydrothermal reaction of a mixture of $H_2$BDC and $Al(NO_3)_3$ $9H_2O$ (1:2 ratio, respectively) heated up to 220 °C for 72 h produced a highly crystalline phase of the as-MIL-53(Al)-BDC (see Supporting Information).[65] Both the as-synthetized materials yielded microcrystalline solids. Prior to $SO_2$ adsorption experiments, the MIL-53(Al)-TDC acetone-exchanged sample was activated at 200 °C under vacuum for 4 h (see Supporting Information). A hydrated-MIL-53(Al)-BDC sample (initially calcined at 230 °C for 3 days in order to remove all the unreacted $H_2$BDC; see Supporting Information) was activated by heating up to 220 °C under vacuum for 6 h. Both activated MIL-53(Al)-BDC and MIL-53(Al)-TDC materials resulted in white microcrystal powders. Their corresponding powder X-ray diffraction (PXRD) patterns (Figures S1 and S2, respectively) correspond to those reported previously by Loiseau *et al.*[53] and Stock *et al.*,[61] respectively. The $N_2$ adsorption experiments revealed BET areas of 1210 and 1260 $m^2$ $g^{-1}$ and pore volumes of 0.51 and 0.45 $cm^3$ $g^{-1}$ for the activated MIL-53(Al)-BDC and MIL-53(Al)-TDC (Figures S3 and S4, respectively), in agreement with previous findings.[61,65]

**2.2. $SO_2$ Adsorption in MIL-53(Al)-TDC.** Figure 1 shows the $SO_2$ adsorption−desorption isotherms for MIL-53(Al)-TDC at 298 K and up to 1 bar. One observes that the adsorption branch exhibits the standard type-I profile for a microporous solid without the presence of steps or inflections points at 298 K (Figure S5). This suggests that this material does not undergo any substantial structural changes upon $SO_2$ adsorption in the range of temperatures explored. From 0 to


https://doi.org/10.1021/acsami.1c09944
ACS Appl. Mater. Interfaces 2021, 13, 39363−39370

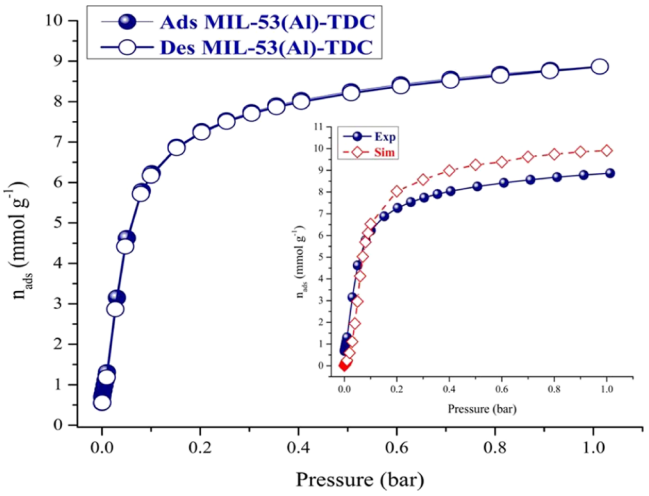


**Figure 1.** Experimental $SO_2$ adsorption−desorption isotherms collected for a fully activated MIL-53(Al)-TDC sample (filled blue circles = adsorption; open blue circles = desorption) at 298 K and up to 1 bar. The inset shows the comparison between the experimental (filled blue circles) and the grand canonical Monte Carlo (GCMC) simulated (open red rhombus) $SO_2$ adsorption isotherms.

0.05 bar, the $SO_2$ capacity sharply increases up to 4.7 mmol $g^{-1}$, an uptake similar to that reported previously for MFM-300(In) and MFM-601(Zr) at similar pressure (5.9 and ∼4.0 mmol $g^{-1}$).[66,67] This is followed by a less-steep increase from 0.05 to 0.2 bar (7.1 mmol $g^{-1}$) and a further gradual increment from 0.2 to 1.0 bar to reach a maximum uptake of 8.9 mmol $g^{-1}$ (Figure 1).

The resulting $SO_2$ saturation capacity is higher than those previously reported for representative MOF materials showing similar pore volume including MIL-160,[44] MFM-300(Al, In),[51,66] Mg-MOF-74,[47] and M-(BDC)(ted)$_{0.5}$ (M = Ni, Zn)[68] (7.2, 8.3, 8.1, and 2.5 mmol $g^{-1}$, respectively) among others (see Table S1). Interestingly, the adsorption and desorption branches coincide, the absence of hysteresis suggesting a full reversibility of the $SO_2$ capture.

The $SO_2$ experimental adsorption isotherm was fairly reproduced by GCMC simulations considering a rigid-like framework for MIL-53(Al)-TDC (Figure 1). The low-pressure regime below 0.2 bar was well captured by our simulations, while the saturation uptake (9.90 mmol $g^{-1}$) was predicted to be slightly higher than the experimental one. In particular, the sudden increase of $SO_2$ uptake below 0.05 bar is attributed to a relatively high $SO_2$/MIL-53(Al)-TDC affinity with an associated simulated adsorption enthalpy at low coverage (−41.0 kJ $mol^{-1}$) in good agreement with the experimentally determined isosteric adsorption enthalpy of −45.6 kJ $mol^{-1}$ (see Supporting Information, Figures S10 and S11).

To gain further insights into the microscopic adsorption behavior of $SO_2$, MC simulations were carried out in the canonical ensemble for different $SO_2$ loadings. At the initial stage of adsorption, $SO_2$ was found to interact *via* its O-atoms with the H-atom of the $\mu$-OH group of MIL-53(Al)-TDC with a mean separating distance of 2.05 Å, as defined by the radial distribution function (RDF) plotted for the corresponding atom pair in Figure S22. Such scenario that remains valid at higher $SO_2$ loading corresponds to relatively strong host/guest interactions, which is reminiscent with what we already reported for $SO_2$ in other MOFs containing hydroxyl groups.[69,70] In addition, the $SO_2$ molecules establish additional weaker interactions with the aromatic rings through their oxygen atoms, with mean separating distances of about 3.5 Å. At higher loading, the $SO_2$ molecules interact with each other with a mean separating distance of about 3.34 Å (Figure S22). An illustration of these interactions and the resulting arrangements of the $SO_2$ molecules is provided in Figure 2a−c at low, intermediate, and saturation loadings, respectively.

We further investigated the regeneration ability of MIL-53(Al)-TDC by performing cycling experiments by only applying vacuum ($1.7 \times 10^{-6}$ Torr for 30 min) at 298 K. This material was shown to exhibit a very good $SO_2$ cyclability with an adsorption capacity preserved after 50 adsorption−desorption cycles, as illustrated in Figure S12. The PXRD pattern of the sample after these adsorption−desorption cycling experiments showed that the integrity of the structure is overall maintained, however, associated with a small loss of crystallinity, as suggested by a moderate broadening of the Bragg peaks (Figure S14). This demonstrates the high stability of MIL-53(Al)-TDC upon exposure to $SO_2$. We further

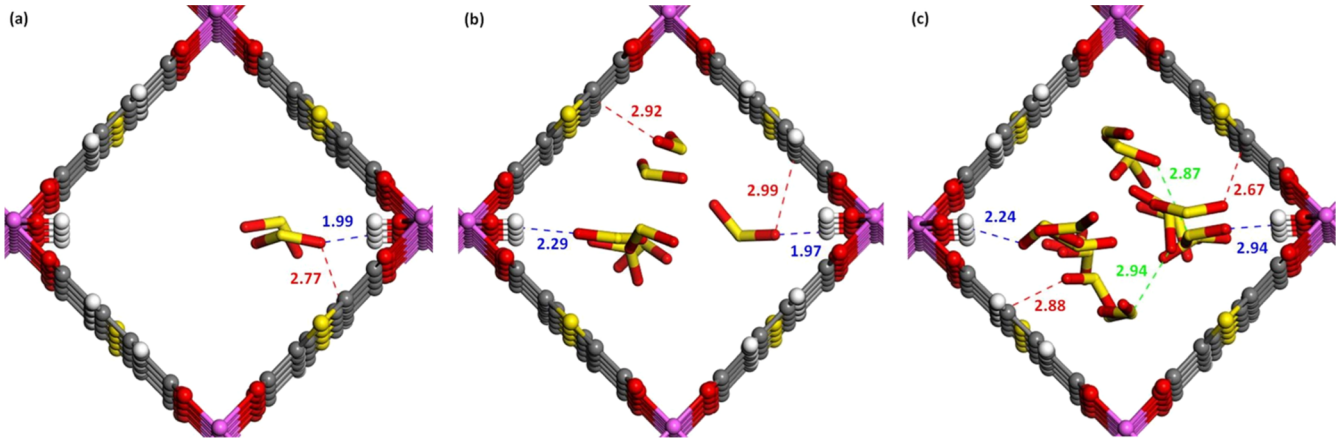


**Figure 2.** Illustrative snapshots of $SO_2$ in the pores of MIL-53(Al)-TDC issued from MC simulations for (a) 1.1 mmol $g^{-1}$ (low loading), (b) 5.0 mmol $g^{-1}$ (intermediate loading), and (c) 9.1 mmol $g^{-1}$ (high loading). Color codes: Al, pink; O, red; S, yellow; C, gray; and H, white. The main interactions are reported as dashed lines, that is, $O_{SO_2}$−$H_{\mu\text{-OH}}$ (blue), $O_{SO_2}$−$C_{org}$ (red), and $S_{SO_2}$−$O_{SO_2}$ (green). The distances are expressed in angstrom.



https://doi.org/10.1021/acsami.1c09944
ACS Appl. Mater. Interfaces 2021, 13, 39363−39370

exposed MIL-53(Al)-TDC to wet $SO_2$ during 24 h using a home-designed setup (Figure S18). The PXRD pattern collected for this sample revealed a retention of the initial crystal structure with a small loss of the crystallinity (Figure S16). This makes MIL-53(Al)-TDC among the few very MOFs stable under this harsh operating condition.[39−41]

**2.3. $SO_2$ Adsorption in MIL-53(Al)-BDC.** Figure 3 reports the $SO_2$ adsorption−desorption isotherms for MIL-53(Al)-BDC at 298 K and up to 1 bar. In sharp contrast with MIL-53(Al)-TDC, the benzene dicarboxylate analogue does not exhibit the standard type-I adsorption isotherm but a step-wise profile (Figures 3 and S6). This behavior is reminiscent to that previously reported for the same solid upon adsorption of various gases/vapors and ascribed to guest-induced structural changes of the framework.[54−60] Herein, two consecutive steps were first observed from 0 to 0.04 bar and from 0.04 to 0.09 bar with corresponding $SO_2$ uptakes of ∼0.6 and ∼0.9 mmol $g^{-1}$, respectively. This is followed by a third one from 0.09 to 0.21 bar associated with a sharp increase of the $SO_2$ uptake, leading to 6.2 mmol $g^{-1}$ at the plateau. Finally, a last step is observed from 0.31 to 0.36 bar with a resulting $SO_2$ uptake of ∼8.2 mmol $g^{-1}$ that further gradually increases with pressure until to reach 10.8 mmol $g^{-1}$ at 1 bar (Figure 3). We further observe that the desorption branch shows a large hysteresis, with a complete reversibility upon once reducing the $SO_2$ pressure, which is associated with the flexibility of MIL-53(Al)-BDC.

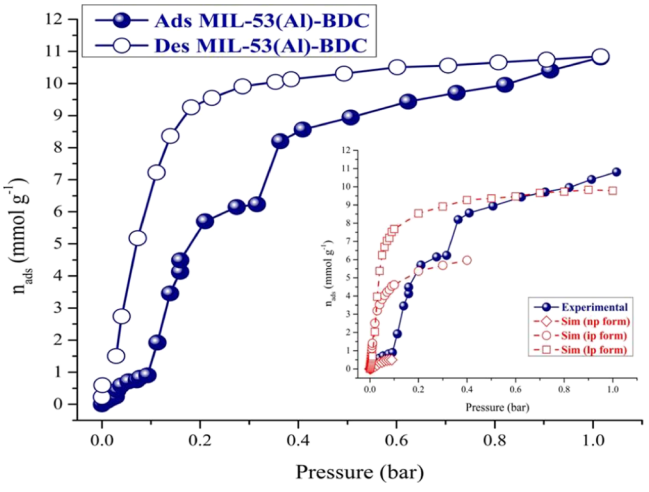


**Figure 3.** Experimental $SO_2$ adsorption−desorption isotherms collected for a fully activated MIL-53(Al)-BDC sample (filled blue circles = adsorption; open blue circles = desorption) at 298 K and up to 1 bar. The inset shows the comparison between the experimental $SO_2$ adsorption isotherm (filled blue circles) and the corresponding GCMC simulated $SO_2$ data (np form: open red rhombus; ip form: open red circles; and lp form: open red squares).

This total $SO_2$ uptake is comparable to other representative MOF materials with relatively larger BET areas and similar pore volume: Mg-MOF-74 (8.6 mmol $g^{-1}$);[47] M(bdc)(ted)$_{0.5}$ (M = Zn 3.0 and Ni 9.9 mmol $g^{-1}$, respectively);[68] M-MFM-300 (M = Al 8.1, In 8.3 and Sc 9.4 mmol $g^{-1}$, respectively);[51,66,71] MFM-202a (10.2 mmol $g^{-1}$);[46] MFM-601 (12.3 mmol $g^{-1}$);[67] and SIFSIX-1-Cu (11.0 mmol $g^{-1}$)[72] (see Supporting Information, Table S1).

Interestingly, this multiple-step adsorption behavior of MIL-53(Al)-BDC deviates with the standard two-step isotherms exhibited by MIL-53(Al or Cr)-BDC[55,73−77] for a wide range of guest molecules including $CO_2$ in MIL-53(Al or Cr)-BDC[55,73−77] at both room and low temperatures, as also confirmed by our own experimental data collected at 298 and 196 K (see Figure S20).

To gain insights into this uncommon guest-induced breathing behavior for MIL-53(Al)-BDC, GCMC-simulated $SO_2$ adsorption isotherms were derived individually for the narrow pore (np) and large pore (lp) forms using the crystal structures preliminarily fully optimized (atomic positions and cell parameters) at the density functional theory (DFT) level in their $SO_2$ loaded forms with 1 and 10.8 mmol $g^{-1}$, respectively, corresponding to the experimental uptakes at low and high pressure (see Supporting Information). Table S7 reports their corresponding DFT-optimized cell parameters. Figure 3 inset shows that the initial stage of adsorption up to 0.1 bar can be well captured by the consideration of the np form, while the lp form allows a good description of the experimental adsorption isotherm at higher pressure above 0.4 bar. An intermediate phase (ip) was further constructed by a fully DFT-optimized lp form preliminarily loaded with 6 mmol $g^{-1}$ of $SO_2$ corresponding to the experimental adsorption uptake at the plateau at 0.3 bar (see Supporting Information for details and Table S7 for the corresponding cell parameters). Figure 3 inset shows that the GCMC-simulated adsorption isotherm for this ip phase well captures the experimental amount adsorbed in the pressure range 0.21−0.3 bar, supporting the existence of a guest-induced intermediate phase in this domain of pressure. The unconventional $SO_2$

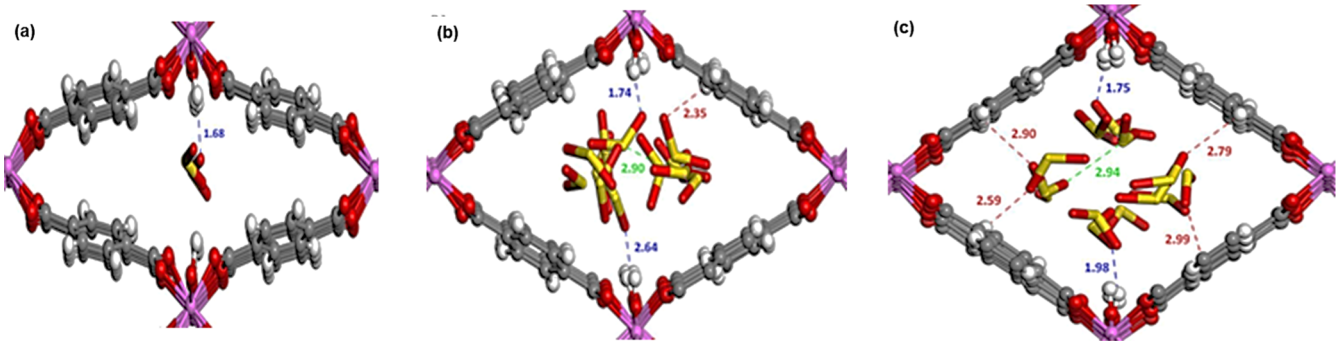


**Figure 4.** Illustrative snapshots of $SO_2$ in the pores of MIL-53(Al)-BDC generated from MC simulations for (a) np form (1 mmol $g^{-1}$), (b) ip form (6 mmol $g^{-1}$), and (c) lp form (9.8 mmol $g^{-1}$). Color codes: Al, pink; O, red; S, yellow; C, gray; and H, white. The main interactions are reported as dashed lines, that is, $O_{SO_2}$−$H_{\mu\text{-OH}}$ (blue), $O_{SO_2}$−$C_{org}$ (red), and $S_{SO_2}$−$O_{SO_2}$ (green); distances are expressed in angstrom.


https://doi.org/10.1021/acsami.1c09944
ACS Appl. Mater. Interfaces 2021, 13, 39363−39370

adsorption isotherm can be thus regarded as a composite isotherm resulting from the contribution of three distinct phases. The existence of three guest-triggered structural changes lp−np, np−ip, and ip−lp during the whole adsorption process is unprecedented for MIL-53(Al, Cr)-BDC, while it is reminiscent to previous findings reported for the initially closed structure of the Fe-analogue upon adsorption of ethane, propane, and butane.[75]

Monte Carlo simulations in the canonical ensemble were further carried out for the np, ip, and lp structures loaded with their respective simulated saturation uptakes. These calculations revealed strong interactions between $SO_2$ molecules *via* their O-atoms and the H-atom of the $\mu$-OH group in the np phase with a mean separating distance of 1.78 Å (see corresponding RDF plots in Figure S23) significantly shorter than in MIL-53(Al)-TDC (2.05 Å, Figure S22) as illustrated in Figure 4a. This trend is consistent with a higher simulated adsorption enthalpy at low coverage ($-50.6$ kJ mol$^{-1}$) *versus* its thiophene analogue ($-41.0$ kJ mol$^{-1}$), also confirmed by the experimental isosteric enthalpy of adsorption at low coverage ($-52.6$ kJ mol$^{-1}$, see Figures S10 and S11). The $SO_2/\mu$-OH interactions remain predominant in the ip and lp phases, although associated with slightly longer distances (Figure S23). Additional interactions also occur between $SO_2$ and the organic linker, as shown in Figure 4b,c. The pore size distributions calculated for all these structures show the following sequence: MIL-53(Al)-TDC > MIL-53(Al)-BDC-lp > MIL-53(Al)-BDC-ip > MIL-53(Al)-BDC-np (7.20, 7.10, 4.80, and 2.80 Å, respectively) (see Figure S24). Indeed, the more confined pores of MIL-53(Al)-BDC-np enable stronger interactions between $SO_2$ and $\mu$-OH (shorter separating distances) as compared to the scenario encountered for the larger pores of MIL-53(Al)-TDC and MIL-53(Al)-BDC-lp, in line with the trend obtained for both experimental and simulated adsorption enthalpy. Since MIL-53(Al)-BDC-ip exhibits an intermediate pore size, the interacting distances between $SO_2$ and $\mu$-OH are in-between those observed for MIL-53(Al)-BDC-np and MIL-53(Al)-BDC-lp.

Continuing with the $SO_2$ adsorption properties, MIL-53(Al)-BDC was demonstrated to exhibit a similar $SO_2$ cyclability to MIL-53(Al)-TDC, with the $SO_2$ capture capacity remaining constant even after 50 adsorption−desorption cycles (Figure S13). Analysis of the PXRD patterns after cycling experiments exhibited that the integrity of the structure is overall maintained, however, associated with a small loss of the crystallinity, as suggested by a moderate broadening of the Bragg peaks for lp-MIL-53(Al)-BDC (Figure S15). Subsequently, an activated sample of lp-MIL-53(Al)-BDC (*vide supra*) was exposed during 24 h to wet $SO_2$, and analysis of the PXRD patterns showed that the sample after being exposed to wet $SO_2$ also retained its crystal structure with a small loss of the crystallinity (Figure S17).

When comparing the $SO_2$ adsorption isotherms of both rigid-like MIL-53(Al)-TDC and flexible MIL-53(Al)-BDC materials (Figure S7), we can observe that (i) at low pressure from 0 to 0.05 bar, MIL-53(Al)-TDC shows a much sharper increase of $SO_2$ uptake (4.7 mmol g$^{-1}$ *vs* 0.6 mmol g$^{-1}$ for MIL-53(Al)-BDC). According to Eddaoudi and co-workers[78] who developed a chemical $SO_2$ sensor using MFM-300(In),[66] MOF structures must meet some general requirements to be applied in the design of $SO_2$ sensor devices, such as high stability to $SO_2$ at room temperature, high capture at low pressure, high affinity, and low reactivation energy.[78−80] In this context, MIL-53(Al)-TDC might be an alternative candidate for $SO_2$ sensing.

(ii) At higher pressure, both materials show relatively high $SO_2$ uptakes combined with outstanding cyclability, keeping their $SO_2$ capture close to the maximum by only applying vacuum to be reactivated. As it was established by Morris and Wheatley,[81] porous solids are becoming a significant technology in gas storage and transportation and two important factors which are considered for their use, that is, a high capture at no-cryogenic conditions and more importantly, soft delivery conditions. Thereby, MIL-53(Al)-TDC and MIL-53(Al)-BDC might be potential candidates for $SO_2$ storage and transportation, which are two application imperatives in fields such as the food industry, fumigation, and petroleum refineries.

## 3. CONCLUSIONS

To summarize, the $SO_2$ adsorption properties of two Al(III)-based MOF materials (MIL-53(Al)-TDC and MIL-53(Al)-BDC) were comprehensively explored. MIL-53(Al)-TDC was demonstrated to act as a rigid-like material upon $SO_2$ adsorption. Conversely, MIL-53(Al)-BDC was shown to exhibit a spectacular guest-induced flexibility of the framework with the presence of multiple steps in the $SO_2$ adsorption isotherm that was attributed to the subsequent existence of three different np, ip, and lp phases along the $SO_2$ pressure, as revealed by molecular simulations. Furthermore, MIL-53(Al)-TDC and MIL-53(Al)-BDC have been demonstrated to be exceptional candidates for the capture of $SO_2$, even under humid conditions, with excellent $SO_2$ uptake, very good cyclability, remarkable chemical stability, and easy regeneration. Interestingly, the $SO_2$-induced flexible behavior of MIL-53(Al)-BDC might open new application avenues such as the $SO_2$ selective sensing as well as $SO_2$ gas storage and transportation.

## ■ ASSOCIATED CONTENT

### Supporting Information

The Supporting Information is available free of charge at https://pubs.acs.org/doi/10.1021/acsami.1c09944.

Experimental details, PXRD patterns after $SO_2$ exposure, isosteric heat of adsorption of $SO_2$, $SO_2$ adsorption−desorption cycles, and $SO_2$ testing under humid conditions, and computational studies (PDF)

## ■ AUTHOR INFORMATION


### Corresponding Authors

**Guillaume Maurin** − *ICGM, Univ. Montpellier, CNRS, ENSCM, 34095 Montpellier, France*; Email: guillaume.maurin1@umontpellier.fr

**Ilich A. Ibarra** − *Laboratorio de Fisicoquímica y Reactividad de Superficies (LaFReS), Instituto de Investigaciones en Materiales, Universidad Nacional Autónoma de México, 04510 México D.F., Mexico*; orcid.org/0000-0002-8573-8033; Email: argel@unam.mx

### Authors

**Alfredo López-Olvera** − *Laboratorio de Fisicoquímica y Reactividad de Superficies (LaFReS), Instituto de Investigaciones en Materiales, Universidad Nacional Autónoma de México, 04510 México D.F., Mexico*

**J. Antonio Zárate** − *Laboratorio de Fisicoquímica y Reactividad de Superficies (LaFReS), Instituto de Investigaciones en Materiales, Universidad Nacional Autónoma de México, 04510 México D.F., Mexico; ICGM, Univ. Montpellier, CNRS, ENSCM, 34095 Montpellier, France*

**Eva Martínez-Ahumada** − *Laboratorio de Fisicoquímica y Reactividad de Superficies (LaFReS), Instituto de Investigaciones en Materiales, Universidad Nacional Autónoma de México, 04510 México D.F., Mexico*

**Dong Fan** − *ICGM, Univ. Montpellier, CNRS, ENSCM, 34095 Montpellier, France;* orcid.org/0000-0003-1873-3416

**Mariana L. Díaz-Ramírez** − *Laboratorio de Fisicoquímica y Reactividad de Superficies (LaFReS), Instituto de Investigaciones en Materiales, Universidad Nacional Autónoma de México, 04510 México D.F., Mexico;* orcid.org/0000-0002-4403-0522

**Paola A. Sáenz-Cavazos** − *Surfaces and Particle Engineering Laboratory (SPEL), Department of Chemical Engineering, Imperial College London, London SW7 2AZ, U.K.*

**Vladimir Martis** − *Surface Measurement Systems, London HA04PE, U.K.*

**Daryl R. Williams** − *Surfaces and Particle Engineering Laboratory (SPEL), Department of Chemical Engineering, Imperial College London, London SW7 2AZ, U.K.; Director of Discovery Space and Professor of Particle Science, Department of Chemical Engineering, Imperial College, Kensington, London SW7 2BY, U.K.;* orcid.org/0000-0001-5626-5903

**Elí Sánchez-González** − *Institute for Integrated Cell-Material Science (WPI-iCeMS), Kyoto University, 606-8501 Kyoto, Japan*

Complete contact information is available at: https://pubs.acs.org/10.1021/acsami.1c09944

### Author Contributions

¶A.L.-O and J.A.Z contributed equally to this work.

### Notes

The authors declare no competing financial interest.

## ■ ACKNOWLEDGMENTS

This work was granted access to the HPC resources of CINES under the allocation A0100907613 made by GENCI. The authors thank Dr. A. Tejeda-Cruz (powder X-ray; IIM-UNAM), PAPIIT-UNAM(IN202820), Mexico, for financial support. A.L.-O. acknowledges a Ph.D. CONACyT grant (733072; 766200). We thank U. Winnberg (Pharma View Consulting SC) for scientific discussions and G. Ibarra-Winnberg for scientific encouragement.

## ■ REFERENCES

(1) U. S Enviromental Protection Agency. *Our Nation's Air*, 2018, Annual report, https://gispub.epa.gov/air/trendsreport/2019/#home.

(2) Matooane, M.; Diab, R. Health Risk Assessment for Sulfur Dioxide Pollution in South Durban, South Africa. *Arch. Environ. Health* **2003**, *58*, 763−770.

(3) Schwartz, J.; Dockery, D. W. Increased Mortality in Philadelphia Associated with Daily Air Pollution Concentrations. *Am. Rev. Respir. Dis.* **1992**, *145*, 600−604.

(4) Liu, F.; Choi, S.; Li, C.; Fioletov, V. E.; McLinden, C. A.; Joiner, J.; Krotkov, N. A.; Bian, H.; Janssens-Maenhout, G.; Darmenov, A. S.; da Silva, A. M. A New Global Anthropogenic $SO_2$ Emission Inventory for The Last Decade: a Mosaic of Satellite-Derived and Bottom-up Emissions. *Atmos. Chem. Phys.* **2018**, *18*, 16571−16586.

(5) West, P. W.; Gaeke, G. C. Fixation of Sulfur Dioxide as Disulfitomercurate (II) and Subsequent Colorimetric Estimation. *Anal. Chem.* **1956**, *28*, 1816−1819.

(6) Dasgupta, P. K.; DeCesare, K. B. Stability of Sulfur Dioxide in Formaldehyde Absorber and Its Anomalous Behavior in Tetrachloromercurate(II). *Atmos. Environ.* **1982**, *16*, 2927−2934.

(7) Gutiérrez Ortiz, F. J.; Vidal, F.; Ollero, P.; Salvador, L.; Cortés, V.; Giménez, A. Pilot-Plant Technical Assessment of Wet Flue Gas Desulfurization Using Limestone. *Ind. Eng. Chem. Res.* **2006**, *45*, 1466−1477.

(8) Andreasen, A.; Mayer, S. Use of Seawater Scrubbing for $SO_2$ Removal from Marine Engine Exhaust Gas. *Energy Fuels* **2007**, *21*, 3274−3279.

(9) Sohn, H. Y.; Kim, B.-S. A New Process for Converting $SO_2$ to Sulfur without Generating Secondary Pollutants through Reactions Involving CaS and $CaSO_4$. *Environ. Sci. Technol.* **2002**, *36*, 3020−3024.

(10) Hanif, M. A.; Ibrahim, N.; Abdul Jalil, A. Sulfur Dioxide Removal: An Overview of Regenerative Flue Gas Desulfurization and Factors Affecting Desulfurization Capacity and Sorbent Regeneration. *Environ. Sci. Pollut. Res.* **2020**, *27*, 27515−27540.

(11) Li, B.; Ma, C. Study on the Mechanism of $SO_2$ Removal by Activated Carbon. *Energy Procedia* **2018**, *153*, 471−477.

(12) Pham, X.-M.; Pham, D. L.; Hanh, N. T.; Dang Thi, T. A.; Thuy Giang, L. N.; Phuong, H. T.; Anh, N. T.; Nhung, H. T.; Le, G. T.; Hoang, M. H.; Van Nguyen, T. An Initial Evaluation on the Adsorption of $SO_2$ and $NO_2$ over Porous $Fe_3O_4$ Nanoparticles Synthesized by Facile Scalable Method. *J. Chem.* **2019**, *2019*, 9742826.

(13) Demirbas, A. Adsorption of Sulfur Dioxide from Coal Combustion Gases on Natural Zeolite. *Energy Sources, Part A* **2006**, *28*, 1329−1335.

(14) Srinivasan, A.; Grutzeck, M. W. The Adsorption of $SO_2$ by Zeolites Synthesized from Fly Ash. *Environ. Sci. Technol.* **1999**, *33*, 1464−1469.

(15) Lin, X.; Hass, K. C.; Schneider, W. F.; Trout, B. L. Chemistry of Sulfur Oxides on Transition Metals I: Configurations, Energetics, Orbital Analyses, and Surface Coverage Effects of $SO_2$ on Pt(111). *J. Phys. Chem. B* **2002**, *106*, 12575−12583.

(16) Lee, Y.-W.; Park, J.-W.; Choung, J.-H.; Choi, D.-K. Adsorption Characteristics of $SO_2$ on Activated Carbon Prepared from Coconut Shell with Potassium Hydroxide Activation. *Environ. Sci. Technol.* **2002**, *36*, 1086−1092.

(17) Maurin, G.; Serre, C.; Cooper, A.; Férey, G. The New Age of MOFs and of Their Porous-Related Solids. *Chem. Soc. Rev.* **2017**, *46*, 3104−3107.

(18) Liu, Y.; Liu, G.; Zhang, C.; Qiu, W.; Yi, S.; Chernikova, V.; Chen, Z.; Belmabkhout, Y.; Shekhah, O.; Eddaoudi, M.; Koros, W. Enhanced $CO_2/CH_4$ Separation Performance of a Mixed Matrix Membrane Based on Tailored MOF-Polymer Formulations. *Adv. Sci.* **2018**, *5*, 1800982.

(19) Wang, T.; Lin, E.; Peng, Y.-L.; Chen, Y.; Cheng, P.; Zhang, Z. Rational Design and Synthesis of Ultramicroporous Metal-Organic Frameworks for Gas Separation. *Coord. Chem. Rev.* **2020**, *423*, 213485.

(20) Chang, N.; Gu, Z.-Y.; Wang, H.-F.; Yan, X.-P. Metal-Organic-Framework-Based Tandem Molecular Sieves as a Dual Platform for Selective Microextraction and High-Resolution Gas Chromatographic Separation ofn-Alkanes in Complex Matrixes. *Anal. Chem.* **2011**, *83*, 7094−7101.

(21) Islamoglu, T.; Chen, Z.; Wasson, M. C.; Buru, C. T.; Kirlikovali, K. O.; Afrin, U.; Mian, M. R.; Farha, O. K. Metal-Organic Frameworks against Toxic Chemicals. *Chem. Rev.* **2020**, *120*, 8130−8160.

(22) Singh, G.; Lee, J.; Karakoti, A.; Bahadur, R.; Yi, J.; Zhao, D.; Albahily, K.; Vinu, A. Emerging Trends in Porous Materials for $CO_2$ capture and Conversion. *Chem. Soc. Rev.* **2020**, *49*, 4360−4404.
(23) Ma, S.; Zhou, H.-C. Gas Storage in Porous Metal−Organic Frameworks for Clean Energy Applications. *Chem. Commun.* **2010**, *46*, 44−53.
(24) Li, Y.; Wen, G. Advances in Metal-Organic Frameworks for Acetylene Storage. *Eur. J. Inorg. Chem.* **2020**, *2020*, 2303−2311.
(25) Meng, J.; Liu, X.; Niu, C.; Pang, Q.; Li, J.; Liu, F.; Liu, Z.; Mai, L. Advances in Metal-Organic Framework Coatings: Versatile Synthesis and Broad Applications. *Chem. Soc. Rev.* **2020**, *49*, 3142−3186.
(26) Nalaparaju, A.; Jiang, J. Ion Exchange in Metal-Organic Framework for Water Purification: Insight from Molecular Simulation. *J. Phys. Chem. C* **2012**, *116*, 6925−6931.
(27) Zhao, S.-N.; Zhang, Y.; Song, S.-Y.; Zhang, H.-J. Design Strategies and Applications of Charged Metal Organic Frameworks. *Coord. Chem. Rev.* **2019**, *398*, 113007.
(28) Masoomi, M. Y.; Morsali, A.; Dhakshinamoorthy, A.; Garcia, H. Mixed-Metal MOFs: Unique Opportunities in Metal-Organic Framework (MOF) Functionality and Design. *Angew. Chem.* **2019**, *131*, 15330−15347.
(29) Kreno, L. E.; Leong, K.; Farha, O. K.; Allendorf, M.; Van Duyne, R. P.; Hupp, J. T. Metal-Organic Framework Materials as Chemical Sensors. *Chem. Rev.* **2012**, *112*, 1105−1125.
(30) Li, H.-Y.; Zhao, S.-N.; Zang, S.-Q.; Li, J. Functional Metal-Organic Frameworks as Effective Sensors of Gases and Volatile Compounds. *Chem. Soc. Rev.* **2020**, *49*, 6364−6401.
(31) Potyrailo, R. A.; Surman, C.; Nagraj, N.; Burns, A. Materials and Transducers toward Selective Wireless Gas Sensing. *Chem. Rev.* **2011**, *111*, 7315−7354.
(32) Allendorf, M. D.; Dong, R.; Feng, X.; Kaskel, S.; Matoga, D.; Stavila, V. Electronic Devices Using Open Framework Materials. *Chem. Rev.* **2020**, *120*, 8581−8640.
(33) Wu, M.-X.; Yang, Y.-W. Metal−Organic Framework (MOF)-Based Drug/Cargo Delivery and Cancer Therapy. *Adv. Mater.* **2017**, *29*, 1606134.
(34) Mendes, R. F.; Figueira, F.; Leite, J. P.; Gales, L.; Almeida Paz, F. A. Metal-Organic Frameworks: A Future Toolbox for Biomedicine? *Chem. Soc. Rev.* **2020**, *49*, 9121−9153.
(35) Xie, Z.; Fan, T.; An, J.; Choi, W.; Duo, Y.; Ge, Y.; Zhang, B.; Nie, G.; Xie, N.; Zheng, T.; Chen, Y.; Zhang, H.; Kim, J. S. Emerging Combination Strategies with Phototherapy in Cancer Nanomedicine. *Chem. Soc. Rev.* **2020**, *49*, 8065−8087.
(36) Yepez, R.; García, S.; Schachat, P.; Sánchez-Sánchez, M.; González-Estefan, J. H.; González-Zamora, E.; Ibarra, I. A.; Aguilar-Pliego, J. Catalytic Activity of HKUST-1 in The Oxidation of Trans-Ferulic Acid to Vanillin. *New J. Chem.* **2015**, *39*, 5112−5115.
(37) Babucci, M.; Guntida, A.; Gates, B. C. Atomically Dispersed Metals on Well-Defined Supports Including Zeolites and Metal-Organic Frameworks: Structure, Bonding, Reactivity, and Catalysis. *Chem. Rev.* **2020**, *120*, 11956−11985.
(38) Rivera-Torrente, M.; Mandemaker, L. D. B.; Filez, M.; Delen, G.; Seoane, B.; Meirer, F.; Weckhuysen, B. M. Spectroscopy, Microscopy, Diffraction and Scattering of Archetypal MOFs: Formation, Metal Sites in Catalysis and Thin Films. *Chem. Soc. Rev.* **2020**, *49*, 6694−6732.
(39) Martínez-Ahumada, E.; Díaz-Ramírez, M. L.; Velásquez-Hernández, M. d. J.; Jancik, V.; Ibarra, I. A. Capture of toxic gases in MOFs: $SO_2$, $H_2S$, $NH_3$ and NOx. *Chem. Sci.* **2021**, *12*, 6772−6799.
(40) Martínez-Ahumada, E.; López-Olvera, A.; Jancik, V.; Sánchez-Bautista, J. E.; González-Zamora, E.; Martis, V.; Williams, D. R.; Ibarra, I. A. MOF Materials for the Capture of Highly Toxic $H_2S$ and $SO_2$. *Organometallics* **2020**, *39*, 883−915.
(41) Lyu, P.; Maurin, G. H2S Stability of Metal-Organic Frameworks: A Computational Assessment. *ACS Appl. Mater. Interfaces* **2021**, *13*, 4813−4822.
(42) Rodríguez-Albelo, L. M.; López-Mayra, E.; Hamad, S.; Ruiz-Salvador, A. R.; Calero, S.; Navarro, J. A. R. Selective Sulfur Dioxide Adsorption on Crystal Defect Sites on an Isoreticular Metal Organic Framework Series. *Nat. Commun.* **2017**, *8*, 14457.
(43) Mounfield, W. P., III; Han, C.; Pang, S. H.; Tumuluri, U.; Jiao, Y.; Bhattacharyya, S.; Dutzer, M. R.; Nair, S.; Wu, Z.; Lively, R. P.; Sholl, D. S.; Walton, K. S. Synergistic Effects of Water and $SO_2$ on Degradation of MIL-125 in the Presence of Acid Gases. *J. Phys. Chem. C* **2016**, *120*, 27230−27240.
(44) Brandt, P.; Nuhnen, A.; Lange, M.; Möllmer, J.; Weingart, O.; Janiak, C. Metal−Organic Frameworks with Potential Application for $SO_2$ Separation and Flue Gas Desulfurization. *ACS Appl. Mater. Interfaces* **2019**, *11*, 17350−17358.
(45) Han, X.; Yang, S.; Schröder, M. Porous Metal−Organic Frameworks as Emerging Sorbents for Clean Air. *Nat. Rev. Chem.* **2019**, *3*, 108−118.
(46) Yang, S.; Liu, L.; Sun, J.; Thomas, K. M.; Davies, A. J.; George, M. W.; Blake, A. J.; Hill, A. H.; Fitch, A. N.; Tang, C. C.; Schröder, M. Irreversible Network Transformation in a Dynamic Porous Host Catalyzed by Sulfur Dioxide. *J. Am. Chem. Soc.* **2013**, *135*, 4954−4957.
(47) Tan, K.; Zuluaga, S.; Wang, H.; Canepa, P.; Soliman, K.; Cure, J.; Li, J.; Thonhauser, T.; Chabal, Y. J. Interaction of Acid Gases $SO_2$ and $NO_2$ with Coordinatively Unsaturated Metal Organic Frameworks: M-MOF-74 (M = Zn, Mg, Ni, Co). *Chem. Mater.* **2017**, *29*, 4227−4235.
(48) Yang, D.-A.; Cho, H.-Y.; Kim, J.; Yang, S.-T.; Ahn, W.-S. $CO_2$ Capture and Conversion Using Mg-MOF-74 Prepared by a Sonochemical Method. *Energy Environ. Sci.* **2012**, *5*, 6465−6473.
(49) Martínez-Ahumada, E.; Díaz-Ramírez, M. L.; Lara-García, H. A.; Williams, D. R.; Martis, V.; Jancik, V.; Lima, E.; Ibarra, I. A. High and Reversible $SO_2$ Capture by a Chemically Stable Cr(III)-Based MOF. *J. Mater. Chem. A* **2020**, *8*, 11515−11520.
(50) Li, L.; Da Silva, I.; Kolokolov, D. I.; Han, X.; Li, J.; Smith, G.; Cheng, Y.; Daemen, L. L.; Morris, C. G.; Godfrey, H. G. W.; Jacques, N. M.; Zhang, X.; Manuel, P.; Frogley, M. D.; Murray, C. A.; Ramirez-Cuesta, A. J.; Cinque, G.; Tang, C. C.; Stepanov, A. G.; Yang, S.; Schröder, M. Post-Synthetic Modulation of The Charge Distribution in a Metal−Organic Framework for Optimal Binding of Carbon Dioxide and Sulfur Dioxide. *Chem. Sci.* **2019**, *10*, 1472−1482.
(51) Yang, S.; Sun, J.; Ramirez-Cuesta, A. J.; Callear, S. K.; David, W. I. F.; Anderson, D. P.; Newby, R.; Blake, A. J.; Parker, J. E.; Tang, C. C.; Schröder, M. Selectivity and Direct Visualization of Carbon Dioxide and Sulfur Dioxide in a Decorated Porous Host. *Nat. Chem.* **2012**, *4*, 887−894.
(52) Zárate, J. A.; Domínguez-Ojeda, E.; Sánchez-González, E.; Martínez-Ahumada, E.; López-Cervantes, V. B.; Williams, D. R.; Martis, V.; Ibarra, I. A.; Alejandre, J. Reversible and Efficient $SO_2$ capture by a Chemically Stable MOF CAU-10: Experiments and Simulations. *Dalton Trans.* **2020**, *49*, 9203−9207.
(53) Loiseau, T.; Serre, C.; Huguenard, C.; Fink, G.; Taulelle, F.; Henry, M.; Bataille, T.; Férey, G. A Rationale for the Large Breathing of the Porous Aluminum Terephthalate (MIL-53) Upon Hydration. *Chem.—Eur. J.* **2004**, *10*, 1373−1382.
(54) Férey, G.; Serre, C.; Devic, T.; Maurin, G.; Jobic, H.; Llewellyn, P. L.; De Weireld, G.; Vimont, A.; Daturi, M.; Chang, J.-S. Why Hybrid Porous Solids Capture Greenhouse Gases? *Chem. Soc. Rev.* **2011**, *40*, 550−562.
(55) Serre, C.; Bourrelly, S.; Vimont, A.; Ramsahye, N. A.; Maurin, G.; Llewellyn, P. L.; Daturi, M.; Filinchuk, Y.; Leynaud, O.; Barnes, P.; Férey, G. An Explanation for the Very Large Breathing Effect of a Metal-Organic Framework during $CO_2$ Adsorption. *Adv. Mater.* **2007**, *19*, 2246−2251.
(56) Ghoufi, A.; Subercaze, A.; Ma, Q.; Yot, P. G.; Ke, Y.; Puente-Orench, I.; Devic, T.; Guillerm, V.; Zhong, C.; Serre, C.; Férey, G.; Maurin, G. Comparative Guest, Thermal, and Mechanical Breathing of the Porous Metal Organic Framework MIL-53(Cr): A Computational Exploration Supported by Experiments. *J. Phys. Chem. C* **2012**, *116*, 13289−13295.
(57) Kolokolov, D. I.; Jobic, H.; Rives, S.; Yot, P. G.; Ollivier, J.; Trens, P.; Stepanov, A. G.; Maurin, G. Diffusion of Benzene in the

Breathing Metal-Organic Framework MIL-53(Cr): A Joint Experimental-Computational Investigation. *J. Phys. Chem. C* **2015**, *119*, 8217−8225.
(58) Hamon, L.; Leclerc, H.; Ghoufi, A.; Oliviero, L.; Travert, A.; Lavalley, J.-C.; Devic, T.; Serre, C.; Férey, G.; De Weireld, G.; Vimont, A.; Maurin, G. Molecular Insight into the Adsorption of H2S in the Flexible MIL-53(Cr) and Rigid MIL-47(V) MOFs: Infrared Spectroscopy Combined to Molecular Simulations. *J. Phys. Chem. C* **2011**, *115*, 2047−2056.
(59) Bourrelly, S.; Moulin, B.; Rivera, A.; Maurin, G.; Devautour-Vinot, S.; Serre, C.; Devic, T.; Horcajada, P.; Vimont, A.; Clet, G.; Daturi, M.; Lavalley, J.-C.; Loera-Serna, S.; Denoyel, R.; Llewellyn, P. L.; Férey, G. Explanation of the Adsorption of Polar Vapors in the Highly Flexible Metal Organic Framework MIL-53(Cr). *J. Am. Chem. Soc.* **2010**, *132*, 9488−9498.
(60) Chanut, N.; Ghoufi, A.; Coulet, M. V.; Bourrelly, S.; Kuchta, B.; Maurin, G.; Llewellyn, P. L. Tailoring the Separation Properties of Flexible Metal-Organic Frameworks Using Mechanical Pressure. *Nat. Commun.* **2020**, *11*, 1216.
(61) Tschense, C. B. L.; Reimer, N.; Hsu, C.-W.; Reinsch, H.; Siegel, R.; Chen, W.-J.; Lin, C.-H.; Cadiau, A.; Serre, C.; Senker, J.; Stock, N. New Group 13 MIL-53 Derivates Based on 2,5-Thiophenedicarboxylic Acid. *Z. Anorg. Allg. Chem.* **2017**, *643*, 1600−1608.
(62) Tannert, N.; Ernst, S.-J.; Jansen, C.; Bart, H.-J.; Henninger, S. K.; Janiak, C. Evaluation of The Highly Stable Metal−Organic Framework MIL-53(Al)-TDC (TDC = 2,5-thiophenedicarboxylate) as a New and Promising Adsorbent for Heat Transformation Applications. *J. Mater. Chem. A* **2018**, *6*, 17706−17712.
(63) González-Martínez, G. A.; Jurado-Vázquez, T.; Solís-Ibarra, D.; Vargas, B.; Sánchez-González, E.; Martínez, A.; Vargas, R.; González-Zamora, E.; Ibarra, I. A. Confinement of $H_2O$ and EtOH to Enhance $CO_2$ Capture in MIL-53(Al)-TDC. *Dalton Trans.* **2018**, *47*, 9459−9465.
(64) Díaz-Ramírez, M. L.; Vargas, B.; Álvarez, J. R.; Landeros-Rivera, B.; Rivera-Almazo, M.; Ramos, C.; Flores, J. G.; Morales, E.; Vargas, R.; Garza, J.; González-Zamora, E.; Martínez, A.; Solís-Ibarra, D.; Ibarra, I. A. Fluorometric detection of iodine by MIL-53(Al)-TDC. *Dalton Trans.* **2020**, *49*, 6572−6577.
(65) Bolinois, L.; Kundu, T.; Wang, X.; Wang, Y.; Hu, Z.; Koh, K.; Zhao, D. Breathing-Induced New Phase Transition in an MIL-53(Al)-$NH_2$ Metal-Organic Framework under High Methane Pressures. *Chem. Commun.* **2017**, *53*, 8118−8121.
(66) Savage, M.; Cheng, Y.; Easun, T. L.; Eyley, J. E.; Argent, S. P.; Warren, M. R.; Lewis, W.; Murray, C.; Tang, C. C.; Frogley, M. D.; Cinque, G.; Sun, J.; Rudić, S.; Murden, R. T.; Benham, M. J.; Fitch, A. N.; Blake, A. J.; Ramirez-Cuesta, A. J.; Yang, S.; Schröder, M. Selective Adsorption of Sulfur Dioxide in a Robust Metal-Organic Framework Material. *Adv. Mater.* **2016**, *28*, 8705−8711.
(67) Carter, J. H.; Han, X.; Moreau, F. Y.; Da Silva, I.; Nevin, A.; Godfrey, H. G. W.; Tang, C. C.; Yang, S.; Schröder, M. Exceptional Adsorption and Binding of Sulfur Dioxide in a Robust Zirconium-Based Metal-Organic Framework. *J. Am. Chem. Soc.* **2018**, *140*, 15564−15567.
(68) Tan, K.; Canepa, P.; Gong, Q.; Liu, J.; Johnson, D. H.; Dyevoich, A.; Thallapally, P. K.; Thonhauser, T.; Li, J.; Chabal, Y. J. Mechanism of Preferential Adsorption of $SO_2$ into Two Microporous Paddle Wheel Frameworks $M(Bdc)(Ted)_{0.5}$. *Chem. Mater.* **2013**, *25*, 4653−4662.
(69) Stock, N. Metal-Organic Frameworks: Aluminium-Based Frameworks. *Encyclopedia of Inorganic and Bioinorganic Chemistry*; Wiley Online Library, 2014, No. iv, pp 1−16.
(70) Rivera-Almazo, M.; Díaz-Ramírez, M. L.; Hernández-Esparza, R.; Vargas, R.; Martínez, A.; Martis, V.; Sáenz-Cavazos, P. A.; Williams, D.; Lima, E.; Ibarra, I. A.; Garza, J. Identification of the Preferential CO and $SO_2$ adsorption Sites within NOTT-401. *Phys. Chem. Chem. Phys.* **2021**, *23*, 1454−1463.
(71) Zárate, J. A.; Sánchez-González, E.; Williams, D. R.; González-Zamora, E.; Martis, V.; Martínez, A.; Balmaseda, J.; Maurin, G.; Ibarra, I. A. High and Energy-Efficient Reversible $SO_2$ Uptake by a Robust Sc(III)-Based MOF. *J. Mater. Chem. A* **2019**, *7*, 15580−15584.
(72) Cui, X.; Yang, Q.; Yang, L.; Krishna, R.; Zhang, Z.; Bao, Z.; Wu, H.; Ren, Q.; Zhou, W.; Chen, B.; Xing, H. Ultrahigh and Selective $SO_2$ Uptake in Inorganic Anion-Pillared Hybrid Porous Materials. *Adv. Mater.* **2017**, *29*, 1606929.
(73) Ramsahye, N. A.; Maurin, G.; Bourrelly, S.; Llewellyn, P. L.; Loiseau, T.; Serre, C.; Férey, G. On the Breathing Effect of a Metal-Organic Framework upon $CO_2$ Adsorption: Monte Carlo Compared to Microcalorimetry Experiments. *Chem. Commun.* **2007**, *31*, 3261−3263.
(74) Salles, F.; Jobic, H.; Ghoufi, A.; Llewellyn, P. L.; Serre, C.; Bourrelly, S.; Férey, G.; Maurin, G. Transport Diffusivity of $CO_2$ in the Highly Flexible Metal-Organic Framework MIL-53(Cr). *Angew. Chem., Int. Ed.* **2009**, *48*, 8335−8339.
(75) Llewellyn, P. L.; Horcajada, P.; Maurin, G.; Devic, T.; Rosenbach, N.; Bourrelly, S.; Serre, C.; Vincent, D.; Loera-Serna, S.; Filinchuk, Y.; Férey, G. Complex Adsorption of Short Linear Alkanes in the Flexible Metal-Organic-Framework MIL-53(Fe). *J. Am. Chem. Soc.* **2009**, *131*, 13002−13008.
(76) Boutin, A.; Coudert, F.-X.; Springuel-Huet, M.-A.; Neimark, A. V.; Férey, G.; Fuchs, A. H. The Behavior of Flexible MIL-53(Al) upon $CH_4$ and $CO_2$ Adsorption. *J. Phys. Chem. C* **2010**, *114*, 22237−22244.
(77) Li, J.-R.; Kuppler, R. J.; Zhou, H.-C. Selective Gas Adsorption and Separation in Metal-Organic Frameworks. *Chem. Soc. Rev.* **2009**, *38*, 1477−1504.
(78) Chernikova, V.; Yassine, O.; Shekhah, O.; Eddaoudi, M.; Salama, K. N. Highly Sensitive and Selective $SO_2$ MOF Sensor: The Integration of MFM-300 MOF as a Sensitive Layer on a Capacitive Interdigitated Electrode. *J. Mater. Chem. A* **2018**, *6*, 5550−5554.
(79) Fine, G. F.; Cavanagh, L. M.; Afonja, A.; Binions, R. Metal Oxide Semi-Conductor Gas Sensors in Environmental Monitoring. *Sensors* **2010**, *10*, 5469−5502.
(80) Wetchakun, K.; Samerjai, T.; Tamaekong, N.; Liewhiran, C.; Siriwong, C.; Kruefu, V.; Wisitsoraat, A.; Tuantranont, A.; Phanichphant, S. Semiconducting Metal Oxides as Sensors for Environmentally Hazardous Gases. *Sens. Actuators, B* **2011**, *160*, 580−591.
(81) Morris, R. E.; Wheatley, P. S. Gas Storage in Nanoporous Materials. *Angew. Chem., Int. Ed.* **2008**, *47*, 4966−4981.


https://doi.org/10.1021/acsami.1c09944
*ACS Appl. Mater. Interfaces* 2021, 13, 39363−39370